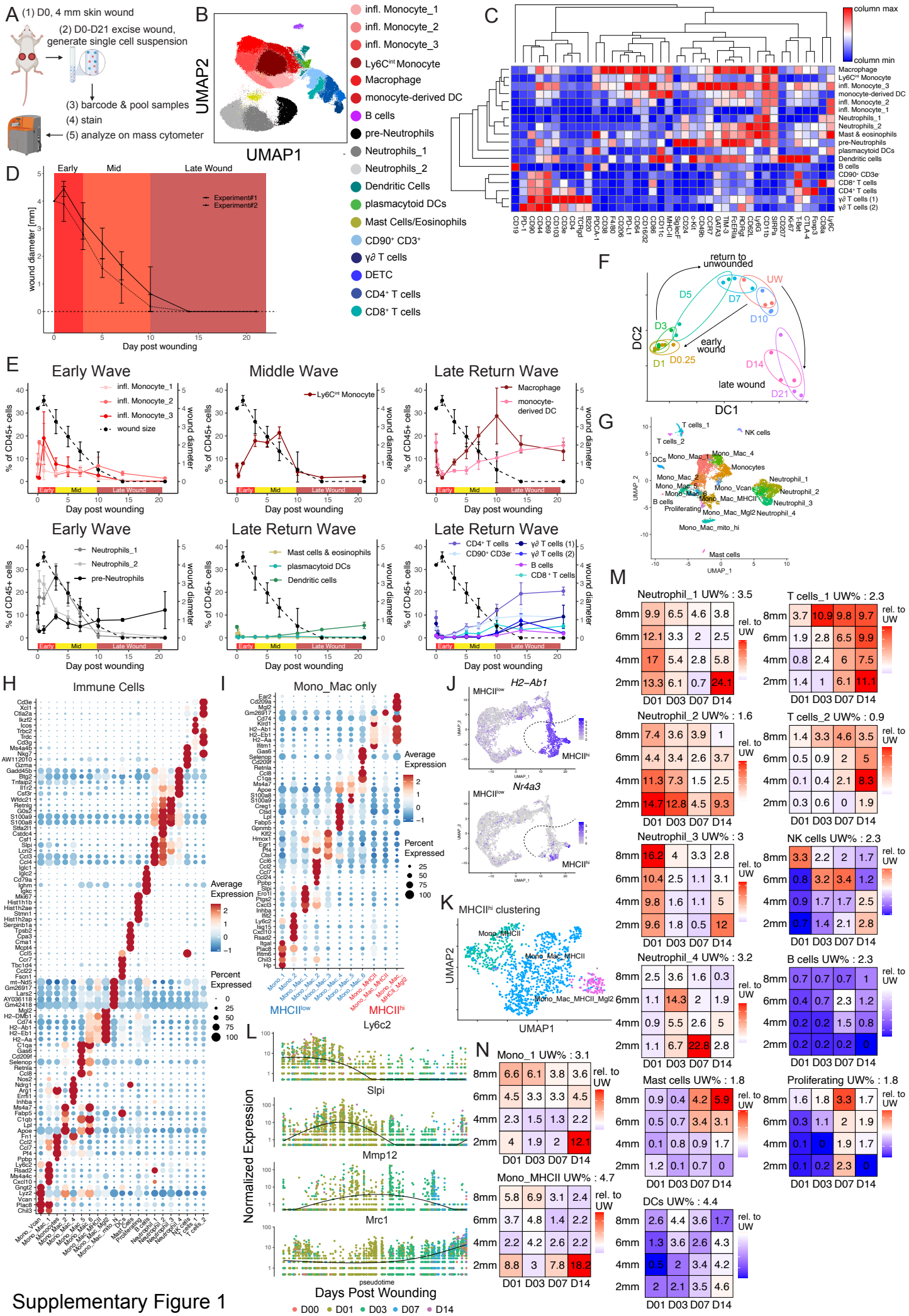

Supplementary Figure 1

Supplementary Figure S1. Separate waves of immune cell infiltration during wound closure, related to Figure 1.

(A) Experimental layout of immune cell profiling during skin wound repair. Four full thickness circular dorsal skin wounds of 4 mm diameter were caused in mice. Wound and surrounding tissue was collected using an 8 mm diameter punch biopsy. A single cell suspension was generated prior to barcoding, staining, and analysis on a mass cytometer and two to four wounds were pooled per mouse. Data in Supplementary Figure S1 represents one of two representative experiments.

(B) UMAP projection of immune cells detected during skin wound repair based on a 40-marker panel.

(**C)** Heatmap of marker expression across all identified cell clusters. Mean intensity of each marker is plotted as scaled value across column.

(D) Diameter of wounds plotted over time of two separate experiments. Each dot represents the mean diameter of 4-12 wounds from 1-3 mice per timepoint. Error bars represent ±SD.

(E) Line plots of all immune cell clusters identified in (B) plotted as percentage of all $CD45^+$ immune cells per timepoint of wound sampling (left y-axis). Dotted line represents wound diameter (right y-axis). Dots represent mean values of n=3 mice per timepoint. Error bars represent ±SD.

(F) Phenotypic earth mover's distance (PhEMD) diffusion map embedding, as described in Chen et al.[41], of all samples collected during wound closure. Each dot represents the wound-resident immune cell composition of one mouse. Dots are color-coded by day and n=3 mice were collected per timepoint. UW, unwounded. DC, diffusion coefficient.

(G) scRNA-Seq UMAP plot of $CD45^+$ immune cells found during skin repair.

(H) Bubble plot of differentially expressed genes across all identified clusters in (G).

(I) Bubble plot of differentially expressed genes across all Mono_Mac subpopulations.

(J) UMAP plot of all monocyte/macrophage cells. Violet color intensity indicates mRNA expression level of *H2-Ab1* (gene encoding structural component of MHCII complex) and *Nr4a3* within each cell.

(K) UMAP plot of $MHCII^{hi}$ Mono_Mac subset.

(L) Gene expression of select genes along pseudotime. D00 represents unwounded skin.

(M) Right: Space-time tile plot representing the non-Mono_MAC $CD45^+$ subpopulations identified in the scRNAseq dataset during wound healing from Figure S1G. Tiles are color-coded relative to unwounded (UW) state of displayed cell subpopulation: red indicates increase, blue indicates decrease, white indicates no change in subpopulation compared to UW.

(N) Space-time tile plots representing the Mono_2 and Mono_MHCII subpopulations within the Mono_Mac object. Tiles are color-coded relative to unwounded (UW) state of displayed cell subpopulation: red indicates increase, blue indicates decrease, white indicates no change in subpopulation compared to UW.

See also Figure 1.

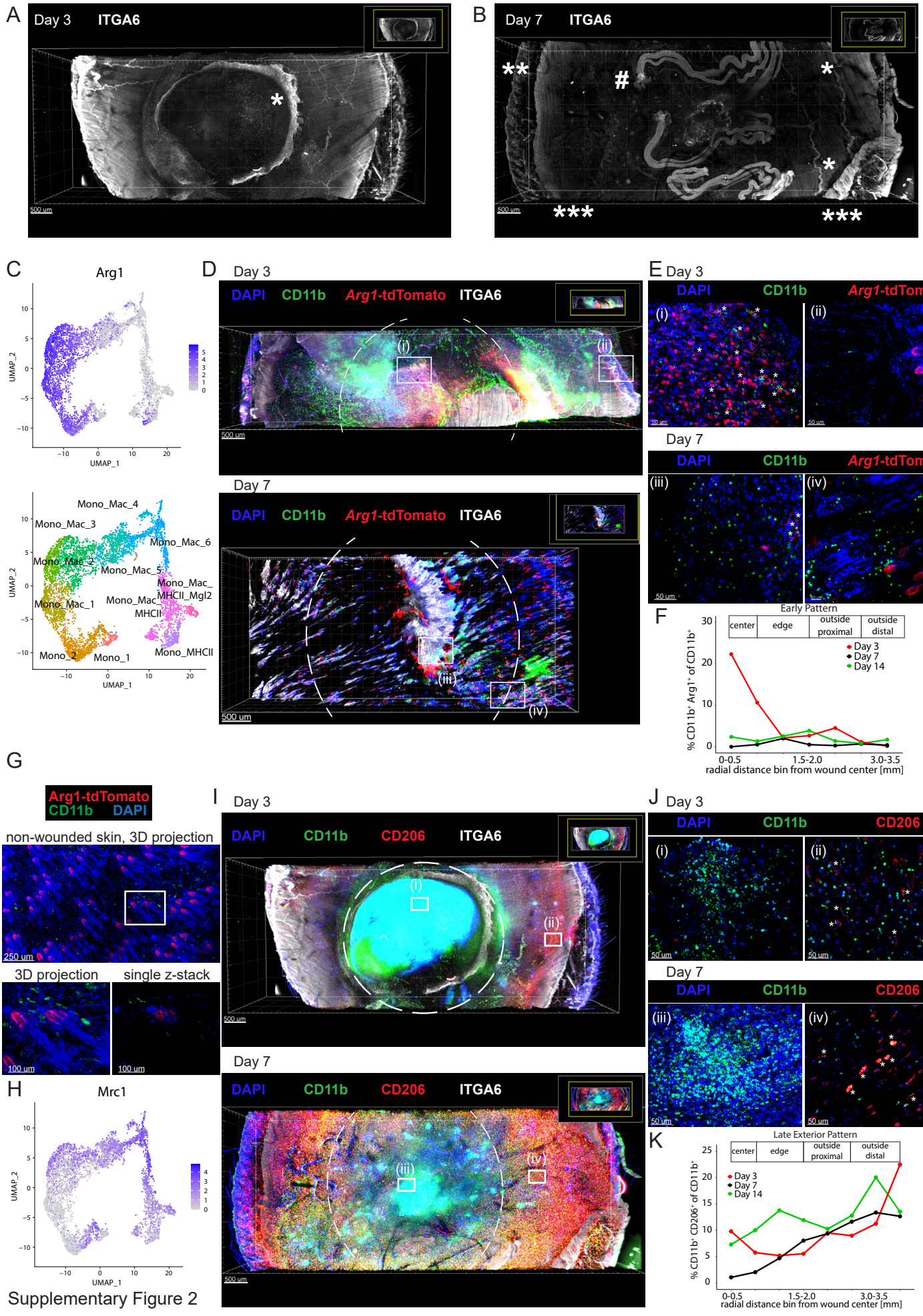

Supplementary Figure 2

Supplementary Figure S2. Whole-mount imaging of wound tissue, related to Figuer 2.

(A) Top-down view of D3 post-wounding imaged sample. Fluorescent stain of CD49f/ITGA6 is shown in white. *Edge of wound with re-established epithelial basement membrane. See Movie S1 for 3D view. One of two representative experiments is shown.

(B) Top-down view of D7 post-wounding imaged sample. Fluorescent stain of CD49f/ITGA6 is shown in white. *Vasculature in non-wounded skin, **hair follicles, ***fascia, #severed nerve bundle. See Movie S2 for 3D view. One of two representative experiments is shown.

(C) Top: UMAP plot of all Mono_Mac clusters. Blue color intensity indicates mRNA expression level of *Arg1* within each cell. Bottom: UMAP plot of Mono_Mac subsets.

(D) Top-down view of stained wound sample from *Arg1*-tdTomato reporter mouse (top) day 3 and (bottom) day 7 post-wounding. Boxes highlight zoom-ins shown in (E). One of two representative images is shown for each day.

(E) Zoom-in of boxes from (D) displaying single z-stack. Images depict wound center region (i) and (iii) or wound distal region (ii) and (iv). $CD11b^+$ *Arg1*-$tdTomato^+$ double-positive cells are highlighted by an asterisk, which are predominantly found in the wound center on day 3. Bar, 50 μm.

(F) Similar to Figure 2E. Quantification of $CD11b^+$ $Arg1^+$ cells relative to distance from the center of the wound from repeat experiment. Percentage of $CD11b^+$ $Arg1^+$ of all $CD11b^+$ are plotted by day post wounding, representing an 'Early Pattern'.

(G) Top-down view of Ce3D-cleared unwounded skin from *Arg1*-reporter mouse stained with antibody against CD11b (green). $Arg1^+$ $CD11b^-$ signal (red) visible in hair follicle bulge. Bottom left, zoomed-in 3D projection of box in top image. Bottom right, single z-stack of zoomed-in region showing no $CD11b^+$ signal in $Arg1^+$ hair follicle bulge.

(H) UMAP plot of all $CD45^+$ immune cells. Blue color intensity indicates mRNA expression level of *Mrc1* within each cell.

(I) Top-down view of stained wound sample from WT mouse (top) day 3 and (bottom) day 7 post-wounding. Boxes highlight zoom-ins shown in (H). One of two representative images is shown for each day.

(J) Zoom-in of boxes from (H) displaying single z-stack. Images depict wound center regions (i) and (iii) or wound distal regions (ii) and (iv). $CD11b^+$ $CD206^+$ double-positive cells are highlighted by an asterisk, which are only found in unwounded skin on day 3 and day 7, and on the wound edge on day 7. Bar, 50 μm.

(K) Similar to Figure 2G. Quantification of $CD11b^+$ $CD206^+$ cells relative to distance from the center of the wound from repeat experiment. Percentage of $CD11b^+$ $CD206^+$ of all $CD11b^+$ are plotted by day post wounding, representing a 'Late Exterior Pattern'.

See also Figure 2.

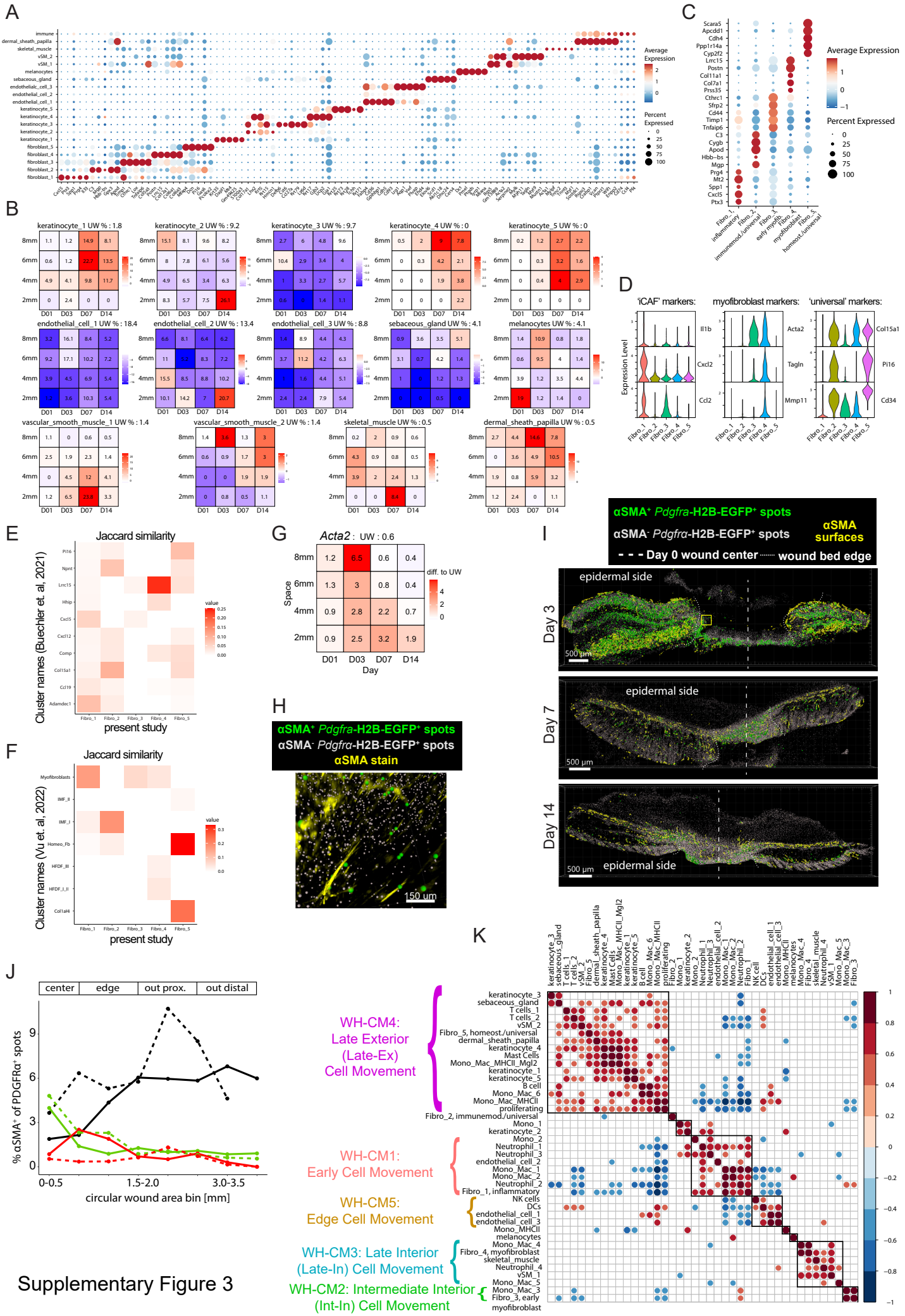

Supplementary Figure 3

Supplementary Figure S3. Identification of non-immune cells in wound scRNAseq data and their relation to immune cells, related to Figure 3.

(A) Bubble plot of differentially expressed genes across all identified $CD45^-$ non-immune cell clusters. Cluster labelled 'immune' expressed high levels of the MHCII invariant chain *Cd74* and was excluded from further analysis.

(B) Space-time tile plots of all $CD45^-$ non-fibroblast non-immune cells identified in the scRNAseq dataset during skin repair. Percentage within all $CD45^-$ non-immune cells is plotted by day and space post-wounding. Tiles are color-coded relative to unwounded (UW) state of displayed cell subpopulation: red indicates increase, blue indicates decrease, white indicates no change in subpopulation compared to UW.

(C) Bubble plot of differentially expressed genes across all fibroblast subpopulations identified during wound skin repair.

(D) Stacked violin plots of select inflammatory cancer-associated fibroblast (iCAF) markers (left), myofibroblast markers (middle), and 'universal' fibroblast markers (right) plotted as natural log-normalized mRNA expression level. Individual violin plots are ordered by fibroblast clusters identified in this study.

(E) Heatmap depicting Jaccard similarity of cluster-specific genes between fibroblast clusters identified in Buechler et al., 2021, and fibroblast subpopulations in present study. About 25% of all differentially expressed genes in Lrrc15 cluster from Buechler et al., 2021, and Fibro_4 cluster in present study were shared.

(F) Heatmap depicting Jaccard similarity of cluster-specific genes between fibroblast clusters identified in Vu et al., 2022, and fibroblast subpopulations in present study. About 30% of all differentially expressed genes in Homeo_Fb cluster from Vu et al., 2022, and Fibro_5 cluster in present study were shared.

(G) Space-time tile plot of *Acta2* (gene encoding for αSMA) mRNA expression (normalized to depth) within all fibroblasts. Tiles are color-coded relative to unwounded (UW) state. Red, high. White, low.

(H) Zoom-in of Ce3D-cleared 250 μm thick section of D3 wounded skin (yellow box) in *Pdgfra*-H2B-$EGFP^{+/WT}$ mice stained with anti-αSMA antibody (yellow). Image was processed to show $αSMA^-$ $Pdgfra^+$ (grey) and $αSMA^+$ $Pdgfra^+$ (green) spots. Scale bar denotes 150 microns.

(I) 3D-views of dorsal skin wound cross-sections from *Pdgfra*-H2B-$EGFP^{+/WT}$ mice collected at (top) day 3, (middle) day 7, and (bottom) day 14 post-wounding. Images were processed to depict $αSMA^+$ *Pdgfra*-H2B-$EGFP^+$ spots in green, $αSMA^-$ *Pdgfra*-H2B-$EGFP^+$ spots in grey, and $αSMA^+$ *Pdgfra*-H2B-$EGFP^-$ surfaces in violet. $αSMA^+$ *Pdgfra*-H2B-$EGFP^-$ surfaces most likely represent vascular smooth muscle cells surrounding blood vessels. Day 0 wound center annotated by dashed vertical line and wound bed edge annotated by dotted line. Images representative of 2 independent experimental replicates. Yellow box on D3 sample represents approximate zoom-in in figure S3U. Scale bar denotes 500 microns.

(J) Quantification of $αSMA^+$ *Pdgfra*-H2B-$EGFP^+$ double-positive spots of all *Pdgfra*-H2B-$EGFP^+$ spots in (I) relative to distance from the center of the wound. Percentage of double-positive $αSMA^+$ *Pdgfra*-H2B-$EGFP^+$ spots are plotted by day post wounding. Data represents two independent replicates with line dashes representing each replicate.

(K) Pearson correlation matrix output of STCA comparing all identified $CD45^+$ immune and $CD45^-$ non-immune cell subpopulations. Dots shown represent statistically significant pairs (p-value<0.05) and color indicates Pearson's correlation coefficient.

See also Figure 3.

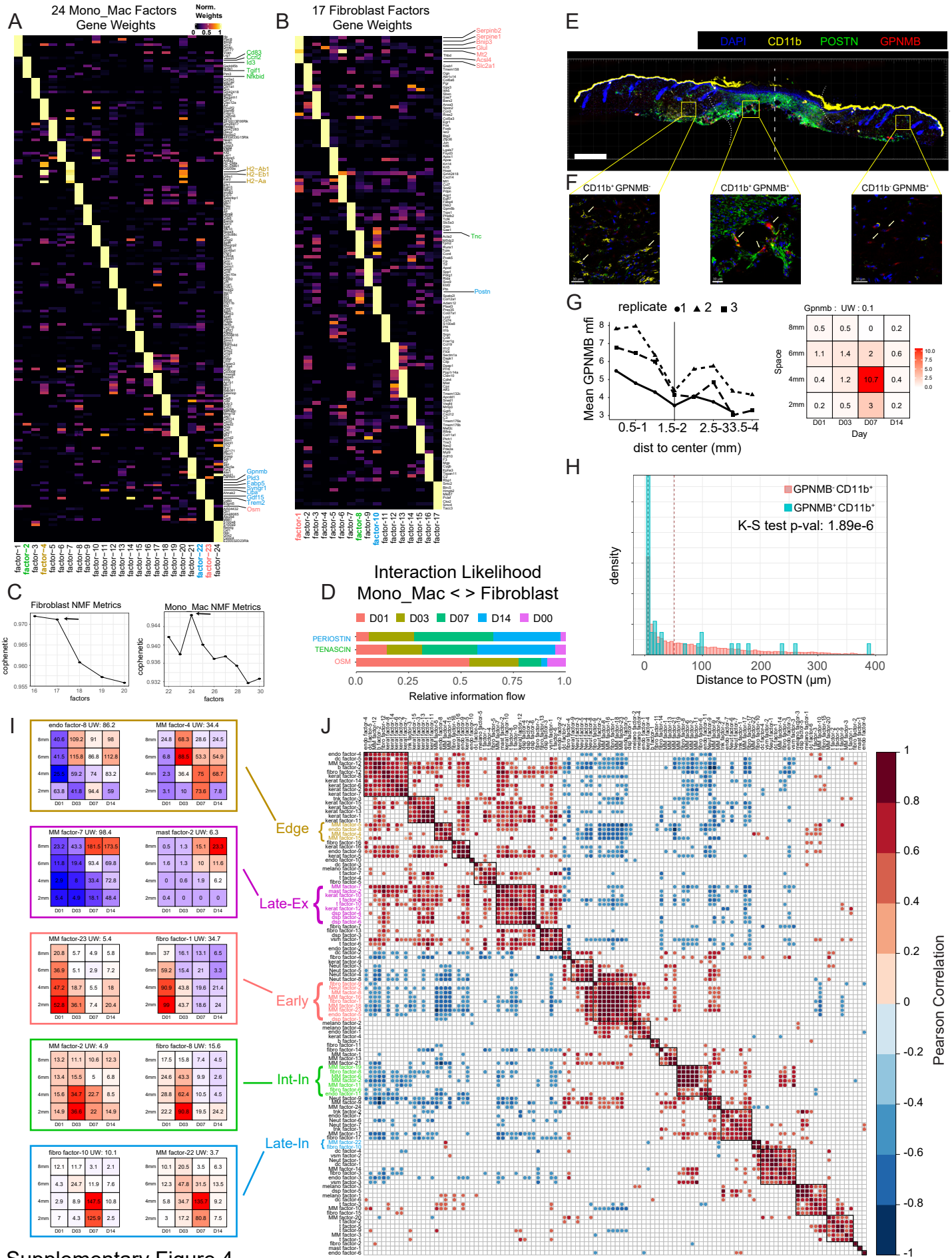

Supplementary Figure 4

Supplementary Figure S4. CellChat and NMF analysis of wound scRNAseq data set, related to Figure 4.

(A) Heatmap showing gene weights for the top 8 contributing genes for each factor in the Mono_Mac subset. Values shown are normalized across the rows such that each gene has a maximal contribution of 1 towards a given factor.

(B) Same analysis as in (A) for the fibroblast subset.

(C) Plot showing strategy for choosing optimal number of factors for NMF decomposition. The factor number prior to a sharp downturn in cophenetic score (stability measure) was chosen.

(D) CellChat stacked bar plot showing relative information flow computed within the Mono_Mac and Fibroblast merged datasets split by timepoint (D00, D1, D3, D7 and D14 following wounding) for the PERIOSTIN, TNC, and OSM pathways.

(E) 3D-views of dorsal skin wound cross-sections collected at (top) day 7 post-wounding showing staining for POSTN, CD11b, and GPNMB. Day 0 wound center annotated by dashed vertical line and approximate wound bed edge annotated by dotted line. Images representative of 3 independent experimental replicates. Scale bar denotes 500 microns.

(F) Inset images focusing on clusters of both GPNMB+ CD11b+ cells and GPNMB- CD11b+ cells and the presence or absence of POSTN signal nearby. Scale bar denotes 20 microns.

(G) Quantification of mean fluorescence intensity of GPNMB staining for CD11b+ cells as a function of distance from the wound center. Line type represents three independent replicates. Accompanying Tileplot denoting mean expression of Gpnmb in the Mono_mac object as a function of space and time in the wound healing scRNA-Seq dataset. Red tiles denote increase relative to the unwounded state while blue tiles denote decrease relative to unwounded skin.

(H) Histogram showing the distribution of distances to the nearest POSTN+ Surface from either GPNMB+ CD11b+ cells or GPNMB-CD11b+ cells. K-S test performed for similarity of distributions. Dotted lines represent the medians of the two distributions.

(I) Tile plots showing average factor loading over space-time for two selected gene programs belonging to the major classes defined (Early/Int-In/Late-In/Late-Ex/Edge) in Figure S4J. are highlighted with matching colors. Red tiles denote increase relative to the unwounded state while blue tiles denote decrease relative to unwounded skin.

(J) Correlation matrix showing the space-time correlation between 114 factors generated from each of the coarse-grained cell type definitions identified in Figures S1J and 4A. Dots shown represent statistically significant pairs (p-value<0.05) and color indicates Pearson's correlation coefficient. Abbreviations: endo, endothelial; dc, dendritic cell; MM, Mono_Mac; fibro, fibroblast; kerat, keratinocyte; tnk, T and NK cell; t, T cell; mast, mast cell; dsp, dermal sheath papilla; vsm, vascular smooth muscle; Neut, neutrophil; melano, melanocyte; b, B cell.

See also Figure 4.

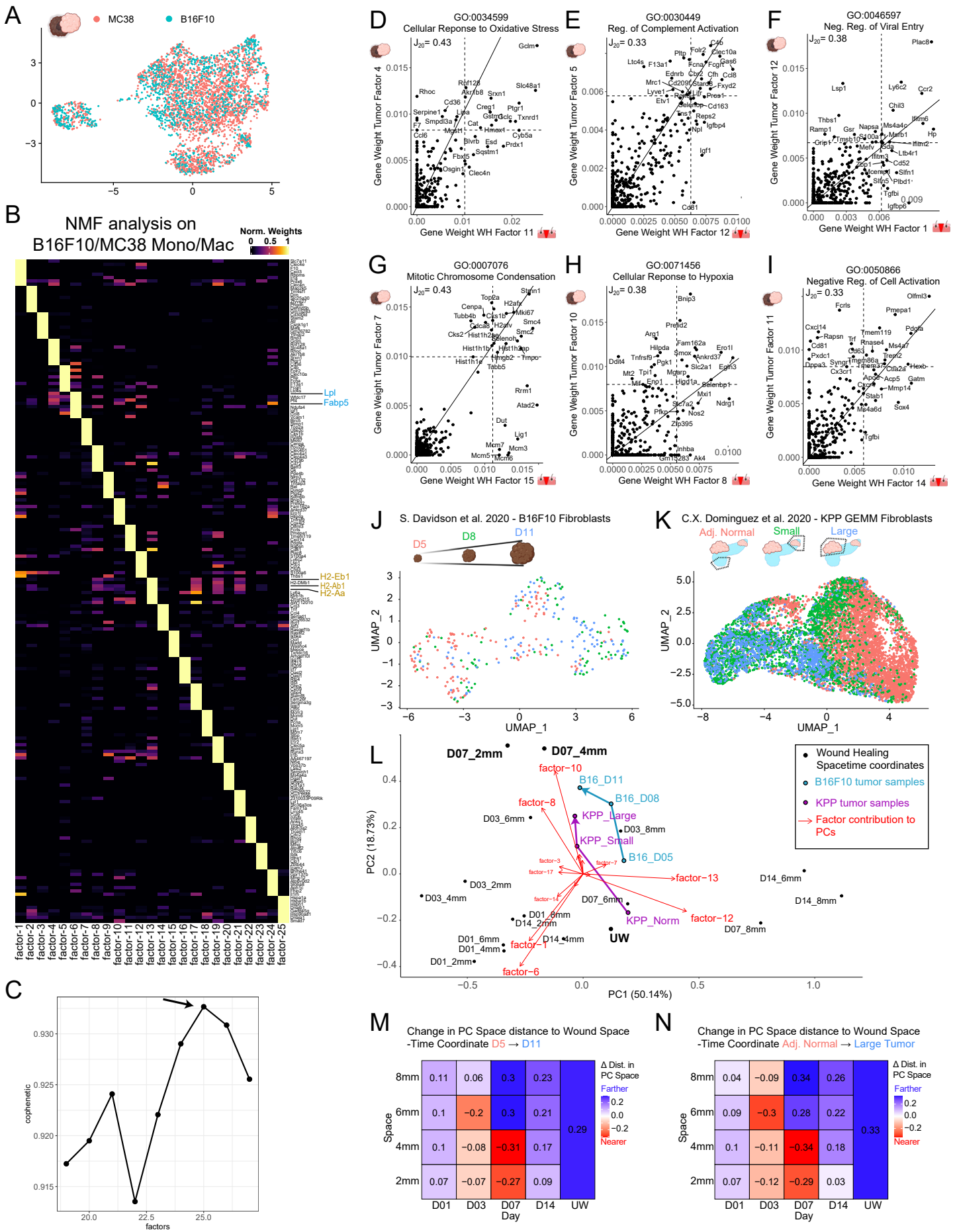

Supplementary Figure 5

Supplementary Figure S5. Translation of mouse wound gene programs to mouse cancer models, related to Figure 5.

(A) UMAP dimensional reduction on integrated MC38 and B16F10 Mono_Mac datasets (n=3859 cells)

(B) Heatmap showing gene weights for the top 8 contributing genes for each factor in the Mono_Mac combined B16F10 and MC38 dataset. Values shown are normalized across the rows such that each gene has a maximal contribution of 1 towards a given factor.

(C) Plot showing strategy for choosing optimal number of factors for NMF decomposition. The factor number prior to a sharp downturn in cophenetic score (stability measure) was chosen.

(D-I) Scatter plots for selected tumor/WH factor pairs for **(D)** Tumor factor-4 vs WH factor-11, **(E)** Tumor factor-5 vs WH factor-12, **(F)** Tumor factor-7 vs WH factor-15, **(G)** Tumor factor-10 and WH factor-8, **(H)** Tumor factor-11 and WH factor-14, and **(I)** Tumor factor-12 and WH factor-1 with the gene weight contributions plotted as calculated from the basis matrix in the NMF output (see Figure S4A for WH factors and S5B for tumor factors). Slope represents x=y line and dotted lines represent the weight for the 20^{th} highest gene contribution in either factor. The $Jaccard_{20}$ index is shown and thus reflects the frequency of points in quadrant I over quadrants I,II and IV. For pairings in **D-I**, top shared genes in the upper right quadrant were put through Enrichr to find overrepresented cellular processes with the top result by p-value listed. Full Enrichr output can be found in the extended data.

(J) UMAP representation of the Fibroblast subset of S. Davidson et al. dataset colored by timepoint (n=316 cells).

(K) UMAP representation of the fibroblasts from C.X. Dominguez et al. 2020, derived from separate samples from the pancreas of a KPP GEMM animal, colored by adj. normal tissue vs. small vs. large tumors (n=8550 cells).

(L) A signature score was generated on the Fibroblast objects in **(J,K)** as well as the wound healing space-time points (17 space-time coordinates) using the top 10 genes contributing to each Mono_mac factor (see **Supp. Figure 5B**). PCA was then performed on these 17 dimensions and each sample plotted in PC space (1^{st} two PCs). Red arrows denote the various factor contributions to these PCs 1+2. Tumor datapoints denoted in blue and purple and wound healing space-time points in black. Arrow between tumor timepoints to highlight tumor stage progression for readability.

(M) Euclidean distances in PC space from B16F10 D5 and D11 samples to each of 17 wound healing space-time coordinates was calculated. Tileplot denotes the change in this distance between D11 and D5 samples. Negative values in red denote the tumor samples approaching that space-time point in PC space, while blue positive values denote distancing.

(N) Euclidean distances in PC space from adjacent normal and large tumor samples from the KPP model to each of 17 wound healing space-time coordinates was calculated. Tileplot denotes the change in this distance between adj. normal and large tumor samples. Negative values in red denote the tumor samples approaching that space-time point in PC space, while blue positive values denote distancing. See also Figure 5.

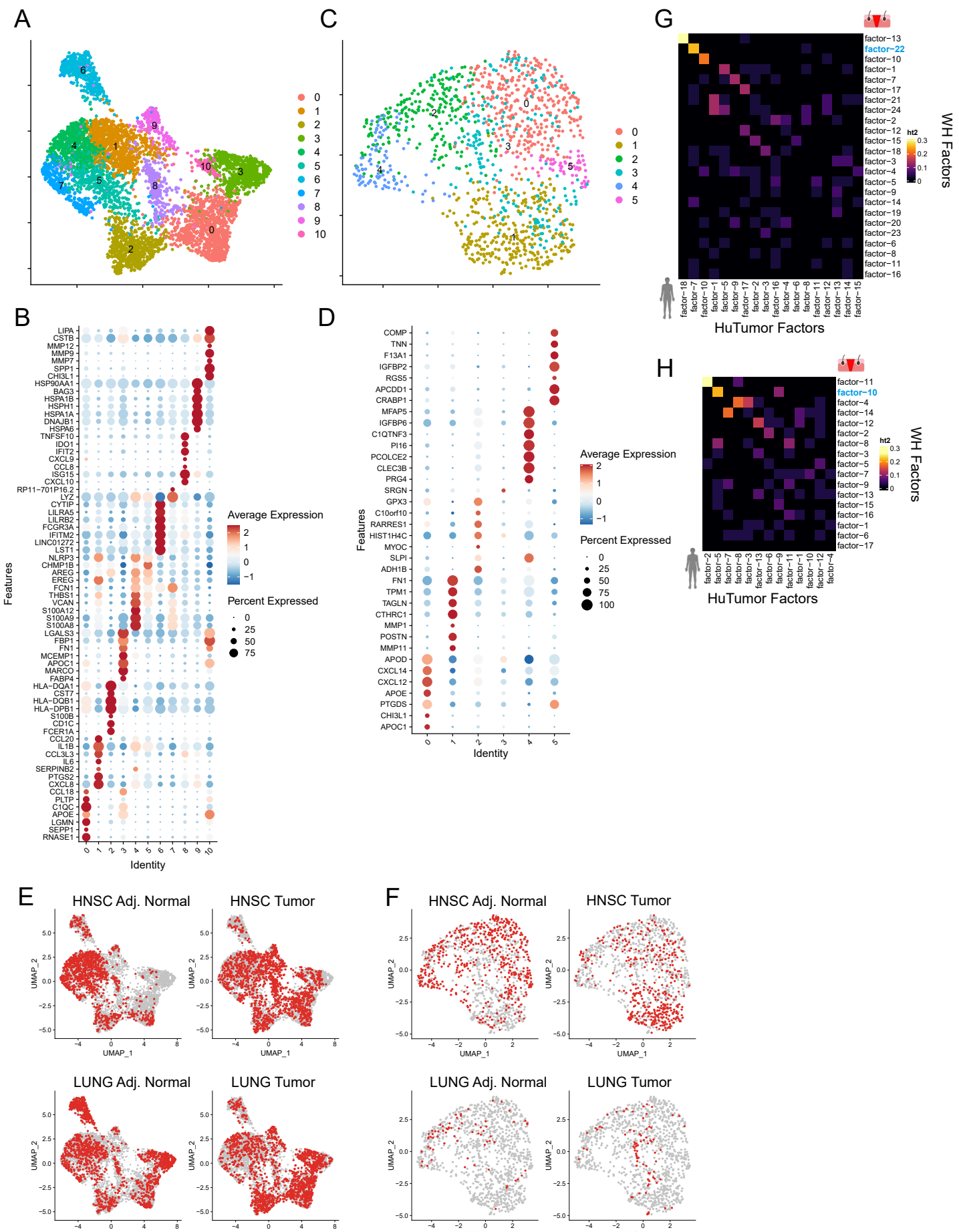

Supplementary Figure 6

Supplementary Figure S6. Translation of mouse wound gene programs to human cancer, related to Figure 6.

(A) Subsetted Mono_Mac object from integrated human tumor scRNA-Seq datasets with cluster numbers denoted in UMAP representation (n=5612 cells).

(B) Dotplot representation of top 7 DE genes for clusters in (N) sorted by log(fold difference) with color representing average expression level and dot size representing the % of cells with a read for the gene.

(C) Subsetted Fibroblast object from integrated human tumor scRNA-Seq datasets with cluster numbers denoted in UMAP representation (n=1263 cells).

(D) Dotplot representation of top 7 DE genes for clusters in (P) sorted by log(fold difference) with color representing average expression level and dot size representing the % of cells with a read for the gene.

(E) UMAP representation of subsetted Mono_Mac object from integrated human tumor scRNA-Seq datasets with cells from different tumor types and either tumor or normal tissue highlighted

(F) UMAP representation of subsetted Fibroblast object from integrated human tumor scRNA-Seq datasets with cells from different tumor types and either tumor or normal tissue highlighted.

(G) Heatmap showing the $Jaccard_{20}$ distance (defined in Materials & Methods) between all 22 M_M wound healing and 18 M_M HuTumor factors based on shared top contributing genes after converting mouse to human gene orthologs.

(H) Heatmap showing the $Jaccard_{20}$ distance (defined in Materials & Methods) between all 17 Fibroblast wound healing and 13 Fibroblast HuTumor factors based on shared top contributing genes after converting mouse to human gene orthologs.

See also Figure 6.

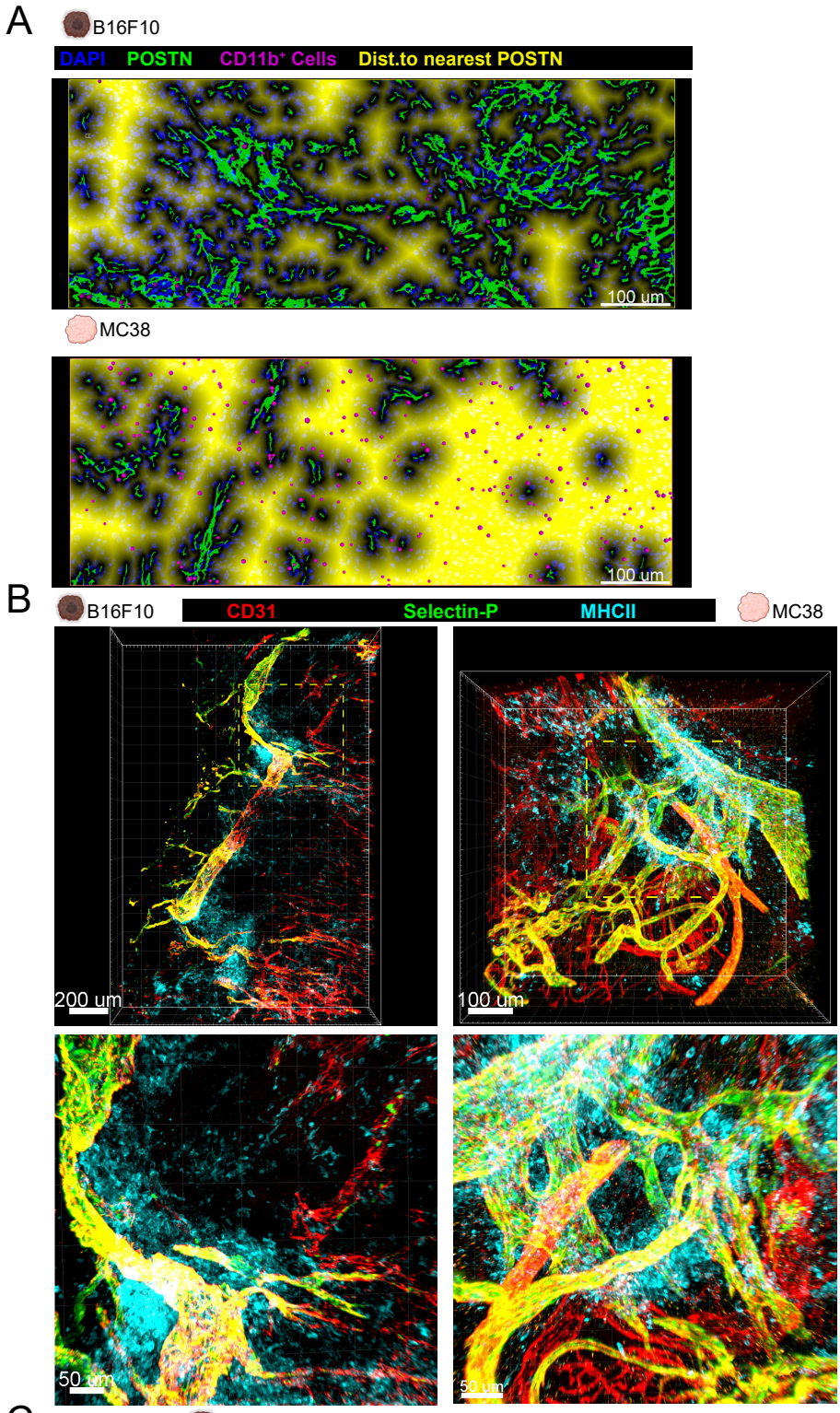

Supplementary Figure 7

Supplementary Figure S7. Imaging of the tumor microenvironment highlights conserved gene program movements, related to Figure 7.

(A) $POSTN^+$ surfaces generated via Imaris overlaid on top of IF images from B16F10 and MC38 tumors. Magenta dots denote $DAPI^+$ spots in close association (within 3 μm) of a $CD11b^+$ surface (defined as $CD11b^+$ Cells) and yellow signal denotes the distance transform from POSTN surfaces. Images representative of 3 separate tumor samples per type.

(B) 3D projections of cleared tissue imaging from 250 μm thick tumor sections from B16F10 and MC38 tumors stained as indicated. Images representative of 4 tumor samples per type.

(C) Histograms indicating the distances of $MHCII^+$ spots and $MHCII^-$ spots to the nearest Selectin-P^+ or Selectin-P^- surface in the MC38 and B16F10 models. Dashed line indicates the median. Histograms representative of 4 independent replicates (4 separate tumors).

See also Figure 7.

Supplementary Table S1.
Table listing cell types and subpopulations according to Space-Time Correlation Analysis (STCA) patterns. vSM, vascular smooth muscle. See also Figures 1, S1, 3, and S3.

Cell Type \ Pattern	WH-CM1: Early	WH-CM2: Int-In, Intermediate Interior	WH-CM3: Late-In, Late Interior	WH-CM4: Late-Ex, Late Exterior	WH-CM5: Edge	Other
Neutrophils	+ Neutrophil_1,2,3	-	+ Neutrophil_4	-	-	-
Mono_Mac	+ Mono_2, Mono_Mac_1,2	+ Mono_Mac_3	+ Mono_Mac_4,5	+ Mono_Mac_6, Mono_Mac_MHCII, Mono_Mac_MHCII_Mgl2	-	+ Mono_1, Mono_MHCII
Fibroblasts	+ Fibro_1, inflammatory	+ Fibro_3, early myofibroblast	+ Fibro_4, myofibroblast	+ Fibro_5, homeostatic/universal	-	+ Fibro_2, immunemodulating/ universal
Keratinocytes	-	-	-	+ keratinocytes_1,3,4,5	-	+ keratinocytes_2
Endothelial	+ endothelial_cell_2	-	-	-	+ endothelial_cell_1,3	-
Mast cells	-	-	-	+	-	-
Dendritic cells	-	-	-	-	+	-
lymphoid	-	-	-	+ B cell, T cells_1,2	+ NK	-
sebaceous gland	-	-	-	+	-	-
dermal sheath papilla	-	-	-	+	-	-
muscle	-	-	+ vSM_1, skeletal muscle	+ vSM_2	-	-
melanocytes	-	-	-	-	-	+ melanocytes